

# Rigidified Derivative of the Non-macrocyclic Ligand H<sub>4</sub>OCTAPA for Stable Lanthanide(III) Complexation

Fátima Lucio-Martínez, Zoltán Garda, Balázs Váradi, Ferenc Krisztián Kálmán, David Esteban-Gómez, Éva Tóth, Gyula Tircsó,\* and Carlos Platas-Iglesias\*



Cite This: <https://doi.org/10.1021/acs.inorgchem.2c00501>



Read Online

ACCESS |



Metrics & More

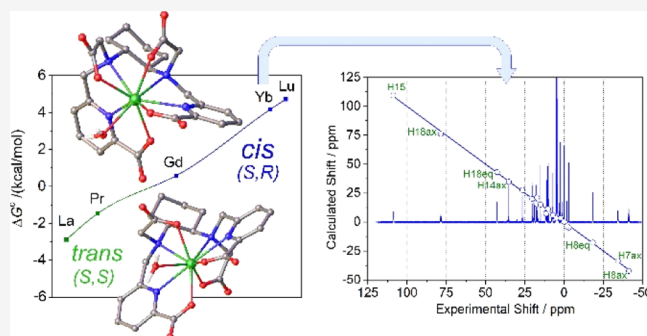


Article Recommendations



Supporting Information

**ABSTRACT:** The stability constants of lanthanide complexes with the potentially octadentate ligand CHXOCTAPA<sup>4-</sup>, which contains a rigid 1,2-diaminocyclohexane scaffold functionalized with two acetate and two picolinate pendant arms, reveal the formation of stable complexes [ $\log K_{LaL} = 17.82(1)$  and  $\log K_{YbL} = 19.65(1)$ ]. Luminescence studies on the Eu<sup>3+</sup> and Tb<sup>3+</sup> analogues evidenced rather high emission quantum yields of 3.4 and 11%, respectively. The emission lifetimes recorded in H<sub>2</sub>O and D<sub>2</sub>O solutions indicate the presence of a water molecule coordinated to the metal ion. <sup>1</sup>H nuclear magnetic relaxation dispersion profiles and <sup>17</sup>O NMR chemical shift and relaxation measurements point to a rather low water exchange rate of the coordinated water molecule ( $k_{ex}^{298} = 1.58 \times 10^6 \text{ s}^{-1}$ ) and relatively high relaxivities of 5.6 and 4.5 mM<sup>-1</sup> s<sup>-1</sup> at 20 MHz and 25 and 37 °C, respectively. Density functional theory calculations and analysis of the paramagnetic shifts induced by Yb<sup>3+</sup> indicate that the complexes adopt an unprecedented cis geometry with the two picolinate groups situated on the same side of the coordination sphere. Dissociation kinetics experiments were conducted by investigating the exchange reactions of LuL occurring with Cu<sup>2+</sup>. The results confirmed the beneficial effect of the rigid cyclohexyl group on the inertness of the Lu<sup>3+</sup> complex. Complex dissociation occurs following proton- and metal-assisted pathways. The latter is relatively efficient at neutral pH, thanks to the formation of a heterodinuclear hydroxo complex.



## INTRODUCTION

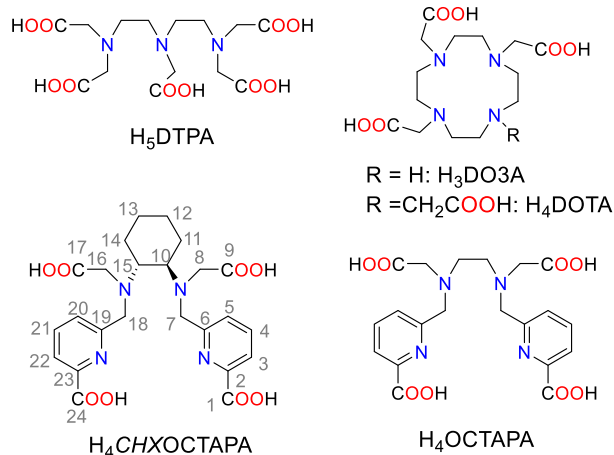
Stable complexation of lanthanide ions (Ln<sup>3+</sup>) in aqueous solution is a coordination chemistry problem that has received much attention in the last 3 decades. This interest is related to a great extent to the important medical and biomedical properties of some lanthanide complexes, which include (1) the use of Gd<sup>3+</sup> complexes as contrast agents in magnetic resonance imaging (MRI),<sup>1–5</sup> (2) the potential of luminescent Ln<sup>3+</sup> complexes, particularly Eu<sup>3+</sup> and Tb<sup>3+</sup>, in optical imaging and bioanalytical applications,<sup>6–8</sup> and (3) the interesting properties of radioisotopes in the lanthanide series (i.e., <sup>177</sup>Lu) for radiopharmaceutical applications.<sup>9,10</sup> All these applications require stable complexation of metal ions and slow dissociation kinetics to avoid undesirable effects (toxicity issues).<sup>11,12</sup> Furthermore, the application of Ln<sup>3+</sup> complexes as radiopharmaceuticals requires a fast complexation of the radioisotope under mild conditions.<sup>13</sup> Chelates for the preparation of efficient luminescent complexes must contain chromophore units suitable for indirect excitation of the relevant Ln<sup>3+</sup> excited state, while protecting the metal ion from the vibrational quenching associated to the coordination of water molecules.<sup>14</sup>

The chelates used for stable Ln<sup>3+</sup> complexes are often either macrocyclic or non-macrocyclic systems containing hard

carboxylate or phosphonate donor groups whose denticity ranges from 7 to 10.<sup>15–17</sup> Ligands with lower denticity like EDTA result in complexes endowed with low stability,<sup>18</sup> while octa- or nonadentate ligands generally present favorable complexation properties.<sup>19,20</sup> Macrocyclic ligands often form complexes with superior thermodynamic stability and exceptional kinetic inertness,<sup>21</sup> but in some cases lead to very slow complexation kinetics.<sup>21–24</sup> On the other hand, non-macrocyclic ligands such as DTPA<sup>5-</sup> (Chart 1) and DTPA bisamides often present faster dissociation kinetics, which is problematic for medical applications.<sup>11,25</sup> Gd<sup>3+</sup> complexes with DTPA bisamides were considered to have superior kinetic inertness than the DTPA<sup>5-</sup> analogue. However, more recent studies demonstrated that different anions present in vivo catalyze the dissociation of Gd<sup>3+</sup> complexes with DTPA bisamides.<sup>11</sup>

Received: February 14, 2022

## Chart 1. Ligands Discussed in the Present Work



In 2004, we reported the potentially octadentate ligand  $\text{H}_4\text{OCTAPA}$  (Chart 1), whose  $\text{Gd}^{3+}$  complex was originally designed as a potential MRI contrast agent candidate.<sup>26</sup> This study demonstrated the presence of a water molecule in the inner coordination sphere. Subsequent investigations performed by Mazzanti,<sup>27,28</sup> Orvig,<sup>29,30</sup> and our own group<sup>31</sup> pointed to a high thermodynamic stability of the lanthanide complexes, which, however, exhibit fast dissociation kinetics. Orvig and co-workers showed that  $\text{OCTAPA}$  presents very promising properties for the development of  $^{111}\text{In}$ ,  $^{90}\text{Y}$ , and  $^{177}\text{Lu}$  radiopharmaceuticals.<sup>32,33</sup> Bifunctional derivatives of  $\text{H}_4\text{OCTAPA}$  were also reported and successfully tested in vivo upon radiolabeling with these radioisotopes.<sup>34–36</sup> The rigidified ligand  $\text{CHXOCTAPA}^{4-}$  (also known as  $\text{H}_4\text{CDDADPA}^{4-}$ ) was reported almost simultaneously by the group of Orvig and us.<sup>37,38</sup> The corresponding  $\text{Gd}^{3+}$  complex is remarkably inert with respect to dissociation, with dissociation rate constants comparable to those of macrocyclic complexes such as  $[\text{Gd}(\text{DO3A})]$ .

In this paper, we present a detailed characterization of the  $\text{Ln}^{3+}$  complexes of  $\text{CHXOCTAPA}$  using a wide range of experimental and computational techniques. A multinuclear ( $^1\text{H}$  and  $^{13}\text{C}$ ) NMR study and density functional theory (DFT) calculations were used to establish the structure of the complexes in solution, including the analysis of the paramagnetic  $\text{Yb}^{3+}$ -induced  $^1\text{H}$  NMR shifts. These studies revealed unexpected features of the structure in solution of these complexes. We also present a full characterization of the relaxometric properties of the  $\text{Gd}^{3+}$  complex involving  $^1\text{H}$  nuclear magnetic relaxation dispersion (NMRD) studies and  $^{17}\text{O}$  NMR chemical shifts and relaxation rates. A detailed analysis of the photophysical properties of the  $\text{Eu}^{3+}$  and  $\text{Tb}^{3+}$  complexes, including quantum yield determination, is reported. Finally, we also determined the stability of some of the complexes across the lanthanide series and assessed their kinetics of dissociation. The stabilities of the complexes formed with divalent metal ions of biological relevance are also reported.

## RESULTS AND DISCUSSION

**Stability of the  $\text{Ln}^{3+}$  Complexes.** Stability constant determination requires measuring the protonation constants of the ligand using the same electrolyte background. The protonation constants of  $\text{CHXOCTAPA}^{4-}$  in 0.15 M NaCl

reported previously by Orvig<sup>37</sup> and us<sup>38</sup> were in good agreement, though slight discrepancies can be noticed for  $\log K_5^{\text{H}}$  and  $\log K_6^{\text{H}}$  (Table S1, Supporting Information). These protonation processes take place in the pH range where complex dissociation occurs, and thus the accurate determination of their values is critical for determining stability constants. We therefore performed new potentiometric titrations using a higher ligand concentration (4.38 mM) in the pH range 1.65–11.95, which allows for a more accurate estimation of protonation constants (Figure S30, Supporting Information). These experiments yielded  $\log K_5^{\text{H}} = 1.59(1)$  and  $\log K_6^{\text{H}} = 0.61(4)$ .

The stability of the  $\text{Gd}^{3+}$  complex with  $\text{CHXOCTAPA}^{4-}$  was reported in a previous paper.<sup>38</sup> This complex was found to be nearly fully formed at  $\text{pH} \sim 2$ , which complicates stability constant determination using potentiometric titrations. The stability of the complex could be determined using the relaxometric method with aqueous solutions buffered with dimethylpiperazine (DMP).<sup>39</sup> Relaxivity,  $r_{1p}$ , refers to the paramagnetic longitudinal relaxation rate enhancement of water protons for a 1 mM concentration of the paramagnetic  $\text{Gd}^{3+}$  ion.<sup>40</sup> The relaxivity of  $[\text{Gd}(\text{H}_2\text{O})_8]^{3+}$  is considerably higher than that of the  $[\text{Gd}(\text{CHXOCTAPA})]^-$  complex, and thus complex dissociation provoked by the addition of competing metal ions ( $\text{La}^{3+}$ ,  $\text{Yb}^{3+}$ , or  $\text{Zn}^{2+}$ ) causes an important increase of the relaxation rate of water protons (Figure 1). These experiments were carried out using the batch

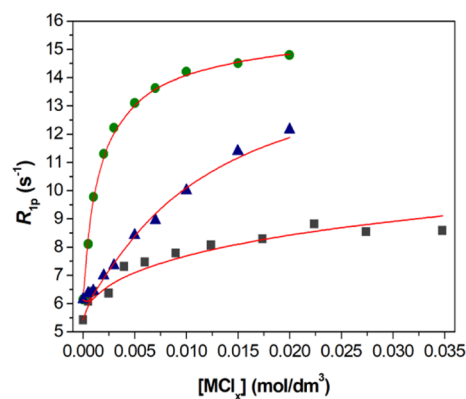


**Figure 1.** Relaxometric titrations (25 °C, 0.15 M NaCl) of the  $[\text{Gd}(\text{CHXOCTAPA})]^-$  complex with  $\text{LaCl}_3$  (squares,  $c_{\text{Lig}} = c_{\text{Gd}^{3+}} = 1.001$  mM at  $\text{pH} = 4.69$ ),  $\text{YbCl}_3$  (circles,  $c_{\text{Lig}} = c_{\text{Gd}^{3+}} = 1.113$  mM at  $\text{pH} = 4.79$ ), and  $\text{ZnCl}_2$  (triangles,  $c_{\text{Lig}} = c_{\text{Gd}^{3+}} = 1.001$  mM at  $\text{pH} = 4.81$ ). All solutions were buffered using 50 mM DMP. The solid lines show the fit of the data for stability constant determination.

method and long equilibration times (4 weeks) to ensure that thermodynamic equilibrium was attained. The titration profiles observed for  $\text{La}^{3+}$  and  $\text{Yb}^{3+}$  are remarkably different, with addition of  $\text{Yb}^{3+}$  inducing a rather sharp inflection point. This anticipates that the stability of the  $\text{Yb}^{3+}$  complex is slightly higher than that of the  $\text{La}^{3+}$  analogue. The fit of the relaxation data confirms this qualitative analysis, yielding stability constants of  $\log K_{\text{YbL}} = 19.60(5)$  and  $\log K_{\text{LaL}} = 18.09(3)$ .

The stability of the complexes with  $\text{CHXOCTAPA}^{4-}$  experiences a slight increase from  $\text{La}^{3+}$  to  $\text{Gd}^{3+}$  as the charge density of the metal ion increases. This is the most common trend observed for  $\text{Ln}^{3+}$  complexes,<sup>41</sup> though it is often more pronounced than observed here.<sup>19</sup> Only a few cases of reversed stability were reported for the complexes of macrocyclic

**Table 1. Protonation and Stability Constants of the Metal Complexes Formed with CHXOCTAPA<sup>4-</sup> and Related Ligands (25 °C, 0.15 M NaCl)**

	CHXOCTAPA <sup>4-</sup>	OCTAPA <sup>4-a</sup>	DTPA <sup>5-</sup>	DO3A <sup>3-g</sup>	DOTA <sup>4-</sup>
log <i>K</i> <sub>LaL</sub>	17.82(1); 18.09(3) <sup>k</sup>	19.92	19.49 <sup>e</sup>	18.63	21.7 <sup>i</sup>
log <i>K</i> <sub>LaHL</sub>	2.00(1)		2.60 <sup>e</sup>		
log <i>K</i> <sub>LaH-1L</sub>	12.75(4)				
log <i>K</i> <sub>GdL</sub>	19.92(1)	20.23	22.03 <sup>d</sup> /22.46 <sup>e</sup>	21.56/19.06 <sup>h</sup>	24.7 <sup>i</sup>
log <i>K</i> <sub>GdHL</sub>	1.02(4)		1.96 <sup>d</sup> /2.39 <sup>e</sup>		
log <i>K</i> <sub>GdH-1L</sub>	12.45(2)				
log <i>K</i> <sub>YbL</sub>	19.65(1), 19.60(5) <sup>k</sup>	19.90 <sup>b</sup>			
log <i>K</i> <sub>YbHL</sub>	1.89(2)				
log <i>K</i> <sub>YbH-1L</sub>	12.24(2)				
log <i>K</i> <sub>LuL</sub>		20.49/20.08 <sup>c</sup>	22.44 <sup>e</sup>	21.44	25.4 <sup>i</sup>
log <i>K</i> <sub>LuHL</sub>			2.18 <sup>e</sup>		
log <i>K</i> <sub>MgL</sub>	5.96(1)	6.12	9.27 <sup>e</sup>	11.64	11.49 <sup>g</sup>
log <i>K</i> <sub>MgHL</sub>	6.03(3)	5.24	6.85 <sup>e</sup>		
log <i>K</i> <sub>MgH2L</sub>		4.54			
log <i>K</i> <sub>CaL</sub>	8.42(2)	9.55/9.4	10.7 <sup>f</sup>	12.57	16.11 <sup>g</sup>
log <i>K</i> <sub>CaHL</sub>	4.83(5)	3.92	6.11 <sup>f</sup>	4.60	
log <i>K</i> <sub>CaH2L</sub>	4.57(6)	2.56			
log <i>K</i> <sub>Ca2L</sub>	3.88(7)	1.55			
log <i>K</i> <sub>ZnL</sub>	16.97(3)	18.91	17.58 <sup>d</sup>	21.57	20.21 <sup>g</sup>
log <i>K</i> <sub>ZnHL</sub>	4.04(3)	3.91	5.37 <sup>d</sup>	3.47	
log <i>K</i> <sub>ZnH2L</sub>	3.15(2)	3.54	2.38 <sup>d</sup>	2.07	
log <i>K</i> <sub>ZnH3L</sub>	1.34(4)				
log <i>K</i> <sub>ZnH-1L</sub>	11.63(7)				
log <i>K</i> <sub>Zn2L</sub>	3.99(5)	2.3	4.33 <sup>d</sup>		
log <i>K</i> <sub>Zn2HL</sub>	3.26(4)				
log <i>K</i> <sub>Zn2L(OH)</sub>	7.63(4)				
log <i>K</i> <sub>Zn2L(OH)2</sub>	8.39(2)				
log <i>K</i> <sub>CuL</sub>	20.76(6) <sup>j</sup>	22.08	23.40 <sup>d</sup>	25.75	24.83 <sup>g</sup>
log <i>K</i> <sub>CuHL</sub>	4.02(9) <sup>j</sup>	3.95	4.63 <sup>d</sup>	3.65	
log <i>K</i> <sub>CuH2L</sub>	4.07(2) <sup>j</sup>	3.21	2.67 <sup>d</sup>	1.69	
log <i>K</i> <sub>CuH3L</sub>			2.03 <sup>d</sup>		
log <i>K</i> <sub>CuH-1L</sub>	12.26(5) <sup>j</sup>				
log <i>K</i> <sub>Cu2L</sub>	5.64(6) <sup>j</sup>	3.2	6.56 <sup>d</sup>		
log <i>K</i> <sub>Cu2HL</sub>	3.33(6) <sup>j</sup>		2.20 <sup>d</sup>		
log <i>K</i> <sub>Cu2L(OH)</sub>	7.80(11) <sup>j</sup>				
log <i>K</i> <sub>Cu2L(OH)2</sub>	9.10(11) <sup>j</sup>				

<sup>a</sup>Data from ref 31 in 0.15 M NaCl unless otherwise indicated. <sup>b</sup>Data in 0.16 M NaCl from ref 29. <sup>c</sup>Data from ref 34. <sup>d</sup>Data in 0.15 M NaCl from ref 20. <sup>e</sup>Data in 0.1 M KCl from ref 45. <sup>f</sup>Data in 0.1 M NaCl from ref 45. <sup>g</sup>Data in 0.1 M KCl from ref 47 unless otherwise stated. <sup>h</sup>Data in 0.15 M NaCl from ref 48. <sup>i</sup>Data in 0.1 M NaCl from ref 49. <sup>j</sup>Data obtained by simultaneous fitting of UV-vis and pH-potentiometry titration data obtained at 1:1 and 2:1 metal-to-ligand ratio. <sup>k</sup>Determined using relaxometric titrations.

ligands.<sup>42-44</sup> The complexes with Gd<sup>3+</sup> and Yb<sup>3+</sup> present very similar stability. The complexes with DTPA<sup>5-</sup> present a similar trend, with an initial increase in stability for the light lanthanide ions, the stability constants becoming nearly constant for the heaviest lanthanides (Table 1).<sup>20,45</sup>

The stability constants determined for the Ln<sup>3+</sup> complexes of CHXOCTAPA<sup>4-</sup> by different methods (pH-potentiometry and <sup>1</sup>H-relaxometry) are in excellent agreement, being comparable with those reported for the analogues with OCTAPA<sup>4-</sup> (Table 1).<sup>29,31</sup> This indicates that the replacement of the ethylenediamine spacer by a more rigid cyclohexyl group does not have a significant impact on complex stability, as observed recently for uranyl complexes.<sup>46</sup> The stability constants characterizing the Ln<sup>3+</sup> complexes of CHXOCTAPA<sup>4-</sup> are similar to those of DO3A<sup>3-</sup>,<sup>47,48</sup> but remain lower than those reported for the analogous DOTA<sup>4-</sup> complexes.<sup>47,49</sup> We note that the stability constants determined in 0.1 M KCl and 0.15 M NaCl for the Gd<sup>3+</sup> complex of DTPA<sup>5-</sup> are in good agreement, while there is

a significant difference in the case of DO3A<sup>3-</sup>. This shows that Na<sup>+</sup> cations form a relatively stable complex with DO3A<sup>3-</sup> derivatives.<sup>48</sup>

Potentiometric titrations using a high ligand concentration (4.38 mM) in the presence of equimolar concentrations of La<sup>3+</sup>, Gd<sup>3+</sup>, and Yb<sup>3+</sup> allowed for determining stability and protonation constants of the metal complexes. The log *K*<sub>LnL</sub> values obtained for the La<sup>3+</sup> and Yb<sup>3+</sup> complexes are in excellent agreement with those obtained by relaxometry. These experiments afforded also the protonation constant of the complexes and also evidenced the formation of hydroxo complexes at high pH (log *K*<sub>LnH-1L</sub> > 12, Figures S7 and S8). For Gd<sup>3+</sup>, the stability constant determined by potentiometry log *K*<sub>GdL</sub> = 19.92(1) is slightly lower than that obtained previously by relaxometry (log *K*<sub>GdL</sub> = 20.68).<sup>38</sup> This slight discrepancy is related to the different set of ligand protonation constants used in the analysis.

The stability constants of the  $\text{Mg}^{2+}$  and  $\text{Ca}^{2+}$  complexes of  $\text{CHXOCTAPA}^{4-}$  could be determined using direct potentiometric titrations. Both cations form different protonated complex species in solution. Similarly, potentiometric titrations, using both 1:1 and 1:2 (M/L) stoichiometric ratios, allowed for determining the protonation constants of the complexes formed with  $\text{Zn}^{2+}$  and  $\text{Cu}^{2+}$ . These metal ions also form relatively stable dinuclear complexes characterized by the corresponding equilibrium constants  $K_{\text{M2L}}$  and different hydroxo complexes at basic pH, yielding rather complex species distributions in solution (Table 1; see also Figures S1–S8, Supporting Information).

The stability constant of the  $\text{Zn}^{2+}$  and  $\text{Cu}^{2+}$  complexes is too high to be determined using direct pH potentiometric titrations, and thus UV–vis spectrophotometric experiments were carried out under acidic pH to determine the stability of the  $\text{Cu}^{2+}$  complex, following the changes of the d–d absorption band at ca. 710 nm with pH (Figure S9, Supporting Information). The stability of the  $\text{Zn}^{2+}$  complex was obtained by competition titration with  $\text{Gd}^{3+}$  using relaxometry. The log  $K_{\text{ML}}$  values characterizing the formation of the  $\text{Ca}^{2+}$ ,  $\text{Zn}^{2+}$  and  $\text{Cu}^{2+}$  complexes with  $\text{CHXOCTAPA}^{4-}$  are 1–2 log  $K$  units lower than those of the corresponding complexes formed with  $\text{OCTAPA}^{4-}$ . This is in contrast to previous studies, which evidenced a gain in complex stability with small metal ions upon incorporation of rigid cyclohexyl groups.<sup>55</sup> This imparts  $\text{CHXOCTAPA}^{4-}$  with a higher selectivity for the  $\text{Ln}^{3+}$  ions than  $\text{OCTAPA}^{4-}$  over potentially competing divalent metal ions in vivo.

**Photophysical Properties.** Ligands containing picolinate moieties were found to act as rather efficient sensitizers of the luminescent emission of  $\text{Eu}^{3+}$  and particularly  $\text{Tb}^{3+}$ .<sup>56–59</sup> Furthermore, picolinate units can be easily functionalized to tune their photophysical properties and provide efficient two-photon absorption.<sup>60–62</sup> Thus, we have investigated the emission spectra of the  $[\text{Ln}(\text{CHXOCTAPA})]^-$  ( $\text{Ln} = \text{Eu}, \text{Tb}$ ) complexes in aqueous solution. The emission spectrum of the  $\text{Eu}^{3+}$  complex is dominated by the  ${}^5\text{D}_0 \rightarrow {}^7\text{F}_2$  ( $\Delta J = 2$ ) transition and presents a rather intense  ${}^5\text{D}_0 \rightarrow {}^7\text{F}_0$  transition (Figure 2). This spectral pattern is typical of  $\text{Eu}^{3+}$  in a coordination environment with a low symmetry.<sup>63</sup> The lifetime of the excited  ${}^5\text{D}_0$  state measured in  $\text{H}_2\text{O}$  solution (598  $\mu\text{s}$ ) is typical of  $\text{Eu}^{3+}$  complexes containing one coordinated water molecule ( $q = 1$ ). Lifetime measurements recorded in  $\text{D}_2\text{O}$  solutions afford a much longer lifetime of 2363  $\mu\text{s}$ , as would be

expected considering the efficient vibrational quenching of  $\text{Eu}^{3+}$  luminescence provoked by O–H oscillators of coordinated water molecules.<sup>50</sup> The use of the empirical relationship proposed by Horrocks gives a  $q$  value of  $1.0 \pm 0.1$ , confirming the presence of a water molecule coordinated to the metal center (Table 2).<sup>50</sup>

The emission spectrum recorded for the  $\text{Tb}^{3+}$  complex presents the  ${}^5\text{D}_4 \rightarrow {}^7\text{F}_J$  transitions expected for this metal ion, with  $J$  ranging from 6 to 3 (Figure S11, Supporting Information). The emission lifetimes of the excited  ${}^5\text{D}_4$  state recorded in  $\text{H}_2\text{O}$  and  $\text{D}_2\text{O}$  provide a  $q$  value of 1.3,<sup>51</sup> in agreement with the results obtained for  $\text{Eu}^{3+}$ .

The emission quantum yields measured for the  $\text{Eu}^{3+}$  (3.4%) and  $\text{Tb}^{3+}$  (11%) complexes were obtained using the corresponding trispicolinate complexes as secondary standards<sup>52,53</sup> and are within the normal range reported for monohydrated chelates containing picolinate units.<sup>56,64,65</sup> Thus, it is surprising that quantum yields one order of magnitude lower were reported by Platas-Iglesias et al. for the  $\text{OCTAPA}^{4-}$  analogues using quinine sulfate as standard (0.3 and 1.9% for  $\text{Eu}^{3+}$  and  $\text{Tb}^{3+}$  respectively).<sup>26</sup> Furthermore, higher quantum yields for the latter complexes were presented in a PhD thesis,<sup>66</sup> suggesting that the values reported by Platas-Iglesias were incorrect. We therefore reexamined the photophysical properties of the complexes with  $\text{OCTAPA}^{4-}$  (Table 2). These studies confirmed that the emission quantum yields of the  $\text{Eu}^{3+}$  and  $\text{Tb}^{3+}$  complexes with  $\text{CHXOCTAPA}^{4-}$  and  $\text{OCTAPA}^{4-}$  are very similar. The emission lifetimes measured for the two families of complexes are also very close, confirming the formation of  $q = 1$  species in solution. The emission spectra recorded for the two  $\text{Eu}^{3+}$  complexes are rather similar, with a comparable splitting of the magnetic dipole  ${}^5\text{D}_0 \rightarrow {}^7\text{F}_1$  transition ( $\sim 140 \text{ cm}^{-1}$ ). We notice that the hypersensitive  $\Delta J = 2$  transition is more intense in  $\text{OCTAPA}^{4-}$  than in  $\text{CHXOCTAPA}^{4-}$ , while the intensity of the magnetic dipole  $\Delta J = 1$  transition remains very similar (Figure 2). This results in  $\Delta J = 2/\Delta J = 1$  intensity ratios of 2.6 and 2.9 for the complexes with  $\text{CHXOCTAPA}^{4-}$  and  $\text{OCTAPA}^{4-}$ , respectively. It has been shown that the relative intensity of these transitions is very sensitive to changes in the metal coordination environment.<sup>67,68</sup> Because the nature of the donor atoms and the number of coordinated water molecules is identical in the two complexes, these results suggest that the two complexes are characterized by somewhat different coordination polyhedra.

Further insights into the sensitization efficiency of  $\text{Eu}^{3+}$  by the picolinate chromophores can be gathered by applying the methodology developed by Werts,<sup>54</sup> which allows for estimating the radiative lifetime of the  $\text{Eu}^{3+}$ -centered emission  $\tau_{\text{Rad}}$ , the metal-centered emission quantum yield  $\Phi_{\text{Eu}}$  and the efficiency of the sensitization process  $\eta_{\text{sen}}$  (Table 2). The results of this analysis show that the observed emission quantum yields are limited by rather low  $\Phi_{\text{Eu}}$  values associated to the quenching effect of the coordinated water molecule and a modest sensitization efficiency.<sup>69–71</sup>

**Structure of the  $\text{Ln}^{3+}$  Complexes in Solution.** The structure of the  $[\text{Ln}(\text{CHXOCTAPA})]^-$  complexes was investigated in  $\text{D}_2\text{O}$  solutions at pH 7.0 using  ${}^1\text{H}$  and  ${}^{13}\text{C}$  NMR spectroscopy. We initiated the study by examining the NMR spectra of the diamagnetic  $\text{La}^{3+}$  and  $\text{Lu}^{3+}$  complexes. The spectra of the  $\text{Lu}^{3+}$  complex are consistent with the presence of a main isomer in solution and a  $\text{C}_1$  symmetry, as it shows 24 proton resonances and the same number of carbon

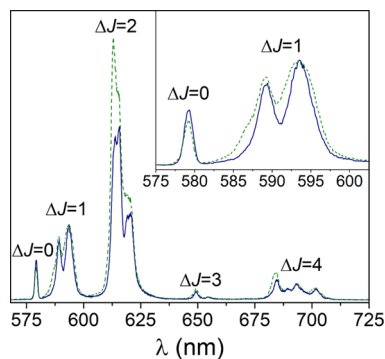


**Figure 2.** Emission spectra of the  $\text{Eu}^{3+}$  complexes with  $\text{CHXOCTAPA}^{4-}$  (blue solid line) and  $\text{OCTAPA}^{4-}$  (green dashed line) recorded in  $\text{H}_2\text{O}$  solution at pH 7.1 ( $\lambda_{\text{ex}} = 279 \text{ nm}$ ; absorption and emission slits 1 nm,  $10^{-4} \text{ M}$ ).

**Table 2.** Spectroscopic Properties of  $[\text{Ln}(\text{CHXOCTAPA})]^-$  and  $[\text{Ln}(\text{OCTAPA})]^-$  Complexes Measured in Aqueous Solutions (pH 7.1)<sup>c</sup>

	$[\text{Eu}(\text{CHXOCTAPA})]^-$	$[\text{Eu}(\text{OCTAPA})]^-$	$[\text{Tb}(\text{CHXOCTAPA})]^-$	$[\text{Tb}(\text{OCTAPA})]^-$
$\lambda_{\text{max}}/\text{nm}$	272	272	271	272
$\epsilon/\text{M}^{-1} \text{cm}^{-1}$	$7.66 \times 10^3$	$7.50 \times 10^3$	$8.34 \times 10^3$	$9.36 \times 10^3$
$\tau_{\text{H}_2\text{O}}/\text{ms}^{\text{a}}$	0.598	0.584	1.527	1.473
$\tau_{\text{D}_2\text{O}}/\text{ms}^{\text{a}}$	2.363	2.292	2.822	2.863
$\Phi_{\text{H}_2\text{O}}/\%^{\text{b}}$	3.4	4.5	11	12
$Q$	1.0	1.1	1.3	1.2
$\tau_{\text{Rad}}/\text{ms}$	6.57	6.07		
$\Phi_{\text{Eu}}/\%$	9.60	9.10		
$\eta_{\text{sens}}$	0.37	0.47		

<sup>a</sup> $\lambda_{\text{exc}} = 279 \text{ nm}$ , estimated error  $\pm 5\%$ ;  $q_{\text{Eu}} = 1.11(\Delta k_{\text{obs}} - 0.31)$ , ref 50;  $q_{\text{Tb}} = 5.0(\Delta k_{\text{obs}} - 0.06)$ , ref 51, with  $(\Delta k_{\text{obs}} = 1/\tau_{\text{H}_2\text{O}} - 1/\tau_{\text{D}_2\text{O}})$ .

<sup>b</sup>Determined using the trispicolinate complexes as standard, refs 52 and 53,  $\lambda_{\text{exc}} = 279 \text{ nm}$ , estimated error  $\pm 15\%$ . <sup>c</sup>Determined according to ref 54.

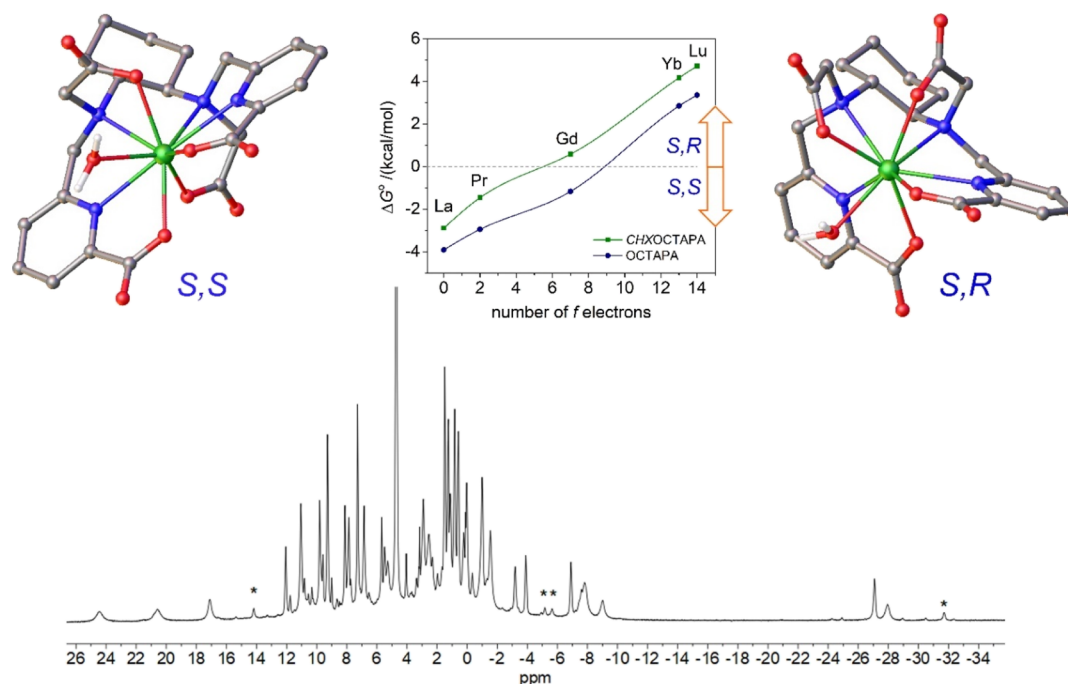


**Figure 3.** Top: Structures of the two isomers of  $[\text{Gd}(\text{CHXOCTAPA})(\text{H}_2\text{O})]^- \cdot 2\text{H}_2\text{O}$  (second-sphere water molecules omitted for clarity) and relative energies calculated across the lanthanide series for the complexes with  $\text{CHXOCTAPA}^{4-}$  and  $\text{OCTAPA}^{4-}$ . Bottom:  $^1\text{H}$  NMR spectrum of the  $\text{Ce}^{3+}$  complex recorded in  $\text{D}_2\text{O}$  solution (300 MHz, 25 °C, pH 7.0). Asterisks denote a minor species present in solution.

signals (Figure S20, Supporting Information). A full attribution of the NMR data was attained with the aid of 2D COSY, HSQC, and HMBC experiments (Table S2, Supporting Information). The spectrum points to a rigid structure of the complex in solution, as the  $^1\text{H}$  spectrum displays well-resolved AB spin systems for the methylene protons. The spectra of the  $\text{La}^{3+}$  complex are, however, more complicated, evidencing the presence of two isomers in solution with very similar populations.

The  $^1\text{H}$  NMR spectrum of the paramagnetic  $\text{Ce}^{3+}$  complex presents paramagnetically shifted signals in the approximate range 25 to  $-35$  ppm (Figure 3). The spectrum is consistent with the presence of two isomers in solution, while only one isomer was observed previously for the  $\text{Eu}^{3+}$  complex.<sup>38</sup> All together, these results indicate that the complexes of the large lanthanide ions ( $\text{La}-\text{Ce}$ ) are present in solution in the form of two diastereoisomers, while only one isomer is observed for  $\text{Eu}^{3+}$  and the heavier  $\text{Ln}^{3+}$  ions. DFT calculations were performed to understand the nature of the two diaster-

eoisomers present in solution for the  $[\text{Ln}(\text{CHXOCTAPA})]^-$  complexes. A careful exploration of the potential energy surface provided two minimum energy geometries with rather small energy differences (Figure 3). These two minimum energy structures differ in the arrangement of the picolinate and acetate groups. One of the structures is characterized by nearly linear angles defined by the two pyridyl N atoms and the metal ion ( $\text{N}_{\text{PY}}-\text{Ln}-\text{N}_{\text{PY}}$ ,  $\sim 170^\circ$ ) and has been denoted as the trans isomer. Conversely, the second isomer (cis) is characterized by the coordination of picolinate (and acetate) groups on the same side of the metal ions, resulting in  $\text{N}_{\text{PY}}-\text{Ln}-\text{N}_{\text{PY}}$  angles of  $\sim 120^\circ$ . The trans isomer is the most stable one at the beginning of the lanthanide series ( $\text{La}-\text{Pr}$ ), while the cis isomer is predicted to be more stable for the second part of the lanthanide series ( $\text{Gd}-\text{Lu}$ ). Analogous calculations performed for the  $[\text{Ln}(\text{OCTAPA})]^-$  complexes provide a similar trend for the relative energies, though the cis isomer is stabilized later on along the series. As a result, our calculations predict that the most stable form for the  $[\text{Gd}(\text{OCTAPA})]^-$  complex is the

trans isomer, which is in nice agreement with the X-ray structure reported by Mazzanti.<sup>27</sup> A trans structure was also established for the light Ln<sup>3+</sup> complexes with OCTAPA<sup>4-</sup> by analysis of the paramagnetic <sup>1</sup>H NMR shifts.<sup>26</sup> The cis isomer is characterized by different configurations of the amine N atoms (S,R or R,S), while these N atoms have the same configuration in the trans isomer (S,S or R,R, Figure 3).

The <sup>1</sup>H NMR spectra of Yb<sup>3+</sup> complexes encode structural information that can be used to validate structural models obtained with DFT calculations.<sup>72</sup> The <sup>1</sup>H NMR signals due to ligand nuclei in paramagnetic Yb<sup>3+</sup> complexes experience large frequency shifts induced by the pseudocontact mechanism ( $\delta^{\text{PC}}$ ), which is related to the anisotropy of the magnetic susceptibility associated to the 4f electrons.<sup>73,74</sup> The pseudocontact shift can be expressed as in eq 1 when the reference frame coincides with the principal directions of the magnetic susceptibility tensor  $\chi$

$$\delta^{\text{PC}} = \frac{1}{12\pi r^3} \left[ \Delta\chi_{\text{ax}} \left( \frac{2z^2 - x^2 - y^2}{r^2} \right) + \frac{3}{2} \Delta\chi_{\text{rh}} \left( \frac{x^2 - y^2}{r^2} \right) \right] \quad (1)$$

where  $r^2 = x^2 + y^2 + z^2$ ,  $x$ ,  $y$ , and  $z$  are the Cartesian coordinates of a nucleus  $i$  relative to the location of a Yb<sup>3+</sup> ion placed at the origin, and  $\Delta\chi_{\text{ax}}$  and  $\Delta\chi_{\text{rh}}$  are the axial and rhombic parameters of the symmetric magnetic susceptibility tensor.

The <sup>1</sup>H NMR spectrum of the Yb<sup>3+</sup> complex of CHXOCTAPA is well resolved, presenting paramagnetically shifted resonances in the range +109 to -41 ppm (Figure 4).

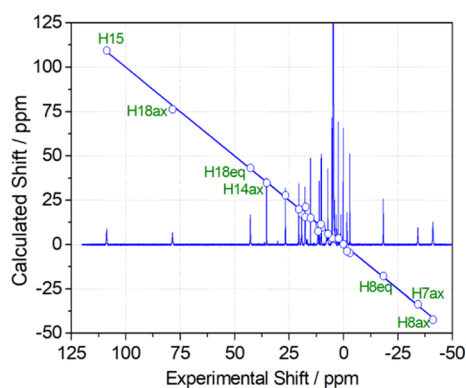


**Figure 4.** <sup>1</sup>H NMR spectrum of [Yb(CHXOCTAPA)]<sup>-</sup> (300 MHz, 25 °C, pH 7.0) and plot of the calculated chemical shifts versus those obtained with eq 1 and the structure of the cis isomer. The line represents the identity line.

The spectrum was assigned on the basis of line-width analysis, as the paramagnetic contribution to the linewidths of <sup>1</sup>H resonances depends on  $1/r^6$ .<sup>75</sup> Thus, those protons located at shorter distances from the paramagnetic ion are characterized by broader resonances. Additional information for the assignment of the <sup>1</sup>H NMR spectrum was gained from <sup>1</sup>H,<sup>1</sup>H-COSY measurements, which show cross-peaks relating the protons of the pyridyl units, the geminal CH<sub>2</sub> protons of the acetate and picolinate groups, and the protons of the cyclohexyl unit placed at a three-bond distance. The analysis of the paramagnetic shifts was accomplished by using eq 1, using the diamagnetic shifts observed for the Lu<sup>3+</sup> analogue (Table S2, Supporting Information). Given the lack of any symmetry axis in the complex, the position of the magnetic axes cannot be anticipated. Thus, we performed a least squares fitting of the

paramagnetic shifts to eq 1 by using five fitting parameters: The axial ( $\Delta\chi_{\text{ax}}/12\pi$ ) and rhombic ( $\Delta\chi_{\text{rh}}/8\pi$ ) parts of the magnetic susceptibility tensor and three Euler angles relating the input orientation and that of the magnetic susceptibility tensor. The structure of the complex obtained with DFT calculations was used as a structural model.

The agreement of the chemical shifts observed for the Yb<sup>3+</sup> complex and those calculated with eq 1 (and the estimates of the diamagnetic shifts using the Lu<sup>3+</sup> complex) is excellent, with deviations <4.2 ppm and a mean deviation of 1.26 ppm (Figure 4, see also Table S2, Supporting Information). This is confirmed by the agreement factor  $AF_i = 0.050$ , which is similar to or better than those reported previously and considered to be satisfactory (0.06–0.11).<sup>76–80</sup> Lower agreement factors were also calculated for symmetrical systems, but in those cases, the fit of the data involved a low number of experimental chemical shifts.<sup>72</sup> This analysis indicates that the structure of the cis isomer obtained with DFT represents a good approximation of the actual structure of the complex in solution. Conversely, an unacceptable fit was obtained by using the trans isomer as the structural model ( $AF_i = 0.363$ ), with deviations of the experimental and calculated data of up to ~34 ppm. As would be expected, the magnetic susceptibility tensor determined for the fit of the data for the cis isomer is rhombic, with  $\Delta\chi_{\text{ax}}/12\pi = -2379 \pm 29$  ppm Å<sup>3</sup> and  $\Delta\chi_{\text{rh}}/8\pi = 919 \pm 65$  ppm Å<sup>3</sup>. The orientation of the magnetic axis is such that one of the picolinate lies close to the  $yz$  plane and one of the carboxylate groups on the  $xz$  plane (Figure S22, Supporting Information).

**<sup>1</sup>H NMRD and <sup>17</sup>O NMR Studies.** The relaxivity of [Gd(CHXOCTAPA)]<sup>-</sup> was investigated in the proton Larmor frequency range 0.01–80 MHz, corresponding to magnetic field strengths varying between  $2.34 \times 10^{-4}$  and 1.88 T (Figure 5). The relaxivities recorded at 20 MHz (Table 3) are slightly higher than those reported for [Gd(OCTAPA)]<sup>-</sup>, [Gd-(DOTA)]<sup>-</sup>, and [Gd(DTPA)]<sup>2-</sup>, but still consistent with the presence of a water molecule in the inner coordination sphere, as indicated by emission lifetime measurements (see above). As expected, fast rotation of the complex in solution limits proton relaxivity, which decreases with increasing temperature. Because the inner-sphere contribution to <sup>1</sup>H relaxivity is affected by a relatively large number of parameters, we have also recorded reduced longitudinal ( $1/T_{1r}$ ) and transverse ( $1/T_{2r}$ ) <sup>17</sup>O NMR relaxation rates and reduced chemical shifts ( $\Delta\omega_r$ ) of an aqueous solution of the complex (19.9 mM, pH = 7.27). These studies provide independent information about some important parameters that control <sup>1</sup>H relaxivity, especially the exchange rate of the coordinated water molecule(s) ( $k_{\text{ex}}^{298}$ ) and the rotational correlation time ( $\tau_R^{298}$ ).<sup>81</sup> The  $1/T_{2r}$  values increase with decreasing temperature at high temperatures, reach a maximum at ca. 322 K, and then decrease. This is typical of systems that experience a changeover from a slow exchange regime at low temperature to a fast exchange condition at high temperature.<sup>82</sup> The inflection point observed for the  $1/T_{2r}$  values is also clearly visible in the chemical shift data.

A simultaneous fitting of the <sup>1</sup>H NMRD and <sup>17</sup>O NMR data of [Gd(CHXOCTAPA)]<sup>-</sup> was performed using a well-established methodology that treats the inner-sphere contribution to relaxivity with the Solomon–Bloembergen–Morgan theory<sup>83–85</sup> and the outer-sphere mechanism with the translational diffusion model proposed by Freed.<sup>86</sup> The <sup>17</sup>O NMR data were fitted with the standard Swift–

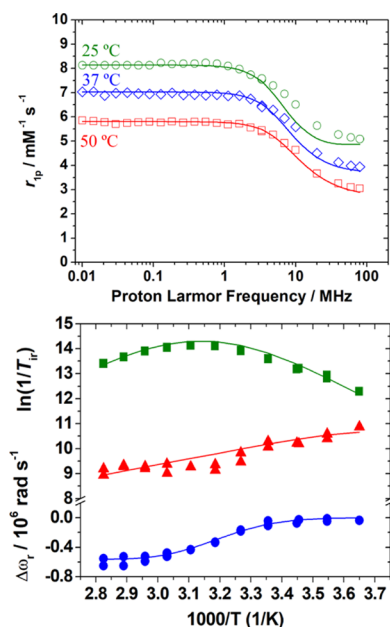


**Figure 5.** Top:  $^1\text{H}$  NMRD profiles recorded at different temperatures for  $[\text{Gd}(\text{CHXOCTAPA})]^-$  (pH 7.27). Bottom: Reduced transverse (green  $\blacksquare$ ) and longitudinal (red  $\blacktriangle$ )  $^{17}\text{O}$  NMR relaxation rates and  $^{17}\text{O}$  NMR chemical shifts (blue  $\bullet$ ) measured for  $[\text{Gd}(\text{CHXOCTAPA})]^-$  at 9.4 T (0.0199 mM, pH = 7.27). The lines represent the fit of the data as explained in the text.

Connick<sup>87,88</sup> equations. Several parameters have been fixed during the fitting procedure: the number of water molecules coordinated to the  $\text{Gd}^{3+}$  ion was fixed to  $q = 1$  on the basis of the luminescence lifetime measurements described above, the distance of closest approach for the outer-sphere contribution  $a_{\text{GdH}}$  was fixed at 3.5 Å, and the distances between the  $\text{Gd}^{3+}$  ion and the H and O atoms of the coordinated water molecule ( $r_{\text{GdH}}$  and  $r_{\text{GdO}}$ ) were set to the values obtained from DFT calculations. The value of the  $^{17}\text{O}$  quadrupole coupling constant  $\chi(1 + \eta^{2/3})^{1/2}$  was also estimated using DFT calculations. In previous studies, the quadrupole coupling constant was allowed to vary during the fitting procedure,<sup>89</sup> providing fitted values that deviated markedly from that

obtained for acidified water (7.58 MHz).<sup>90</sup> As a result, the fits of the data gave low rotational correlation times  $\tau_{\text{R}}$  (Table 3). However, it has been demonstrated that coordination to  $\text{Gd}^{3+}$  provokes negligible changes in the quadrupole constant.<sup>91</sup> Our calculations provided  $\chi = 7.77$  MHz and an asymmetry parameter  $\eta = 0.84$  ( $\chi = 6.68$  MHz and  $\eta = 0.93$  for pure water), yielding a  $\chi(1 + \eta^{2/3})^{1/2}$  value of 10.7 MHz. Additional parameters that were fixed to reasonable values were the diffusion coefficient  $D_{\text{GdH}}^{298}$  ( $20 \times 10^{-10} \text{ m}^2 \text{ s}^{-1}$ ), its activation energy  $E_{\text{DGdH}}$  (22  $\text{kJ mol}^{-1}$ ), and the activation energy for the modulation of the zero field splitting interaction ( $E_{\text{v}} = 1 \text{ kJ mol}^{-1}$ ). The rotational correlation time  $\tau_{\text{R}}$  affects both the  $T_1$   $^{17}\text{O}$  relaxation rates and  $r_{1\text{p}}$  values. However, it has been shown that rotational correlation time characterizing the  $\text{Ln}-\text{H}_{\text{water}}$  vector is  $\sim 65\%$  shorter than that of the  $\text{Ln}-\text{O}_{\text{water}}$  vector.<sup>92</sup> Thus, we included in the fitting two different  $\tau_{\text{R}}$  values with the constraint that  $\tau_{\text{RH}}/\tau_{\text{RO}} = 0.65$ .

An excellent fit of the  $^{17}\text{O}$  NMR and  $^1\text{H}$  NMRD data was obtained using the parameters listed in Table 3. The water exchange rate  $k_{\text{ex}}^{298}$  is lower than those determined for the complexes with  $\text{OCTAPA}^{4-}$  and  $\text{DTPA}^{5-}$ . A faster average exchange rate was also determined for the complexes with  $\text{DOTA}^{4-}$ , though in the latter case two isomers with very different water exchange parameters are present in solution.<sup>93</sup> The rigidity of the  $\text{CHXOCTAPA}^{4-}$  ligand likely increases the energy cost required to reach the transition state responsible for the water exchange process, resulting in a rather low water exchange rate.<sup>94</sup> A similar effect was observed previously upon rigidification of  $\text{OCTAPA}$  derivatives incorporating phosphonate groups.<sup>95</sup> The parameters characterizing the relaxation of the electron spin are very similar to those obtained for  $\text{OCTAPA}^{4-}$ , as would be expected from the similar relaxivities observed at low magnetic fields ( $< 1$  MHz). Complexes with  $\text{DOTA}^{4-}$  derivatives display slower electron spin relaxation, as a result of lower squared zero field splitting energies ( $\Delta^2$ , Table 3). Finally, the value obtained for the hyperfine coupling constant  $A/\hbar$  is in excellent agreement with that estimated with DFT ( $3.10 \times 10^6 \text{ rad s}^{-1}$ ), which provides support to the reliability of the analysis.

**Dissociation Kinetics.** The slow dissociation of  $\text{Ln}^{3+}$  complexes is a key property for their application as both

**Table 3.** Parameters Obtained from the Simultaneous Analysis of  $^{17}\text{O}$  NMR and  $^1\text{H}$  NMRD Data

	$\text{CHXOCTAPA}^{4-}$	$\text{OCTAPA}^{4-b}$	$\text{DTPA}^{5-c}$	$\text{DOTA}^{4-c}$
$r_{1\text{p}}$ at 25/37 °C, 20 MHz/mM $^{-1} \text{ s}^{-1}$	5.6/4.5	5.0/3.9	4.7/4.0	4.7/3.8
$k_{\text{ex}}^{298}/10^6 \text{ s}^{-1}$	$1.58 \pm 0.09$	5.0	3.3	4.1
$\Delta H^\ddagger/\text{kJ mol}^{-1}$	$54.6 \pm 1.8$	40.1	51.6	49.8
$\tau_{\text{RH}}^{298}/\text{ps}$	$75 \pm 3$	55 <sup>b</sup>	58 <sup>b</sup>	77
$E_{\text{v}}/\text{kJ mol}^{-1}$	$19.5 \pm 1.2$	17.9	17.3	16.1
$\tau_{\text{v}}^{298}/\text{ps}$	$11.3 \pm 0.06$	12.6	25	11
$E_{\text{v}}/\text{kJ mol}^{-1}$	1.0 <sup>a</sup>	1.0 <sup>a</sup>	1.6	1.0 <sup>a</sup>
$\Delta^2/10^{20} \text{ s}^{-2}$	$1.04 \pm 0.06$	1.2	0.46	0.16
$D_{\text{GdH}}^{298}/10^{-10} \text{ m}^2 \text{ s}^{-1}$	20.0 <sup>a</sup>	19	20	22
$E_{\text{DGdH}}/\text{kJ mol}^{-1}$	22 <sup>a</sup>	30.1	19.4	20.2
$A/\hbar/10^6 \text{ rad s}^{-1}$	$-3.06 \pm 0.08$	-2.31	-3.8	-3.7
$\chi(1 + \eta^{2/3})^{1/2}/\text{MHz}$	10.7 <sup>a</sup>	17 <sup>b</sup>	14 <sup>b</sup>	10
$r_{\text{GdH}}/\text{Å}$	3.005 <sup>a</sup>	2.969 <sup>a</sup>	3.1 <sup>a</sup>	3.1 <sup>a</sup>
$r_{\text{GdO}}/\text{Å}$	2.480 <sup>a</sup>	2.54 <sup>a</sup>	2.5 <sup>a</sup>	2.5 <sup>a</sup>
$a_{\text{GdH}}/\text{Å}$	3.5 <sup>a</sup>	3.4 <sup>a</sup>	3.5 <sup>a</sup>	3.5 <sup>a</sup>
$q^{298}$	1 <sup>a</sup>	1 <sup>a</sup>	1 <sup>a</sup>	1 <sup>a</sup>

<sup>a</sup>Parameters fixed during the fitting procedure. <sup>b</sup>Data from ref 26. <sup>c</sup>Data from ref 89.

MRI contrast agents and radiopharmaceuticals. In the case of MRI contrast agents, there is an increasing concern on potential toxicity issues related to the release of  $\text{Gd}^{3+}$  in vivo.<sup>96</sup> Radiopharmaceuticals are injected in low doses, and thus chemical toxicity problems are likely not an important concern. However, complex dissociation may have negative effects by reducing the amount of radioisotope that reaches the desired target, thereby exposing to radiation healthy tissue.<sup>97</sup> In a previous paper, we analyzed the dissociation kinetics of the  $\text{Gd}^{3+}$  complex, which was found to be remarkably inert.<sup>38</sup> Herein, we present a detailed analysis of the dissociation kinetics of the  $\text{Lu}^{3+}$  analogue, given the potential of  $^{177}\text{Lu}$  for therapeutic applications. We have shown recently that the dissociation kinetics of  $\text{Ln}^{3+}$  complexes may vary by several orders of magnitude across the lanthanide series, and thus the remarkable inertness of the  $\text{Gd}^{3+}$  complex does not necessarily ensure that the  $\text{Lu}^{3+}$  analogue behaves in a similar way.<sup>98</sup>

The dissociation of the  $\text{Lu}^{3+}$  complex with  $\text{CHXOCTAPA}^{4-}$  was investigated by following the rates of exchange reactions taking place with  $\text{Cu}^{2+}$  at different proton concentrations (pH 3.30–4.72). The reactions were monitored in the presence of at least 10-fold  $\text{Cu}^{2+}$  excess to ensure pseudo first-order conditions. The observed rate constants display a rather unusual behavior, as increasing  $c_{\text{H}^+}$  provokes a slight initial decrease of the dissociation rates, which subsequently increase at higher  $c_{\text{H}^+}$  values. Furthermore,  $\text{Cu}^{2+}$  is also affecting significantly the complex dissociation rates (Figure 6). This

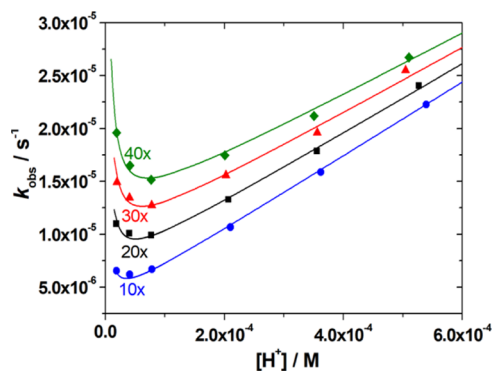


**Figure 6.** Plot of the pseudo-first-order rate constants measured for the  $[\text{Lu}(\text{CHXOCTAPA})]^-$  as a function of  $\text{H}^+$  ion concentration (50 mM DMP, 25 °C, 0.15 M NaCl) using different metal ion excess [10× (5.53 mM), 20× (11.07 mM), 30× (16.60 mM), and 40× (22.14 mM)] with pH = 3.30, 3.50, 3.80, 4.17, and 4.49. The solid lines represent the fits of the data to eq 7.

indicates that the  $\text{Lu}^{3+}$  complex experiences dissociation by following the proton-assisted and metal-assisted pathways, the latter involving formation of a hetero-dinuclear complex. The dinuclear complex appears to form a hydroxo complex at relatively low pH that is responsible for the increase in  $k_{\text{obs}}$  values in the low proton concentration side (Figure 6). Thus, the dissociation of the complex can be expressed as in eq 2, where  $k_0$  is the rate constant characterizing the spontaneous dissociation,  $k_{\text{H}}$  is the rate constant characterizing the proton-assisted dissociation, and  $k_{\text{Cu}}$  and  $k_{\text{Cu}}^{\text{OH}}$  are associated with the metal-assisted dissociation pathways, the latter with the formation of a hydroxo dinuclear complex.

$$-\frac{d[\text{Lu}(\text{L})]_t}{dt} = k_{\text{obs}}[\text{Lu}(\text{L})]_t \\ = k_0[\text{Lu}(\text{L})] + k_{\text{H}}[\text{Lu}(\text{HL})] \\ + k_{\text{Cu}}[\text{Lu}(\text{L})\text{Cu}] + k_{\text{Cu}}^{\text{OH}}[\text{Lu}(\text{L})\text{Cu}(\text{OH})] \quad (2)$$

Considering that the total concentration of complexed  $\text{Lu}^{3+}$  is given by eq 3 and the equilibrium constants defined by eqs 4–6, the rate constants can be expressed as in eq 7, where  $k_1 = k_{\text{H}} \times K_{\text{H}}$ ,  $k_3^{\text{Cu}} = k_{\text{Cu}}K_{\text{Cu}}$ , and  $k_6^{\text{Cu}} = k_{\text{Cu}}^{\text{OH}}K_{\text{Cu}}K_{\text{Cu}(\text{OH})}$ .

$$[\text{Lu}(\text{L})]_t = [\text{LuL}] + [\text{Lu}(\text{HL})] + [\text{Lu}(\text{L})\text{M}] \\ + [\text{Lu}(\text{L})\text{MOH}] \quad (3)$$

$$K_{\text{H}} = \frac{[\text{Lu}(\text{HL})]}{[\text{LuL}][\text{H}^+]} \quad (4)$$

$$K_{\text{Cu}} = \frac{[\text{Lu}(\text{L})\text{Cu}]}{[\text{Lu}(\text{L})][\text{Cu}^{2+}]} \quad (5)$$

$$K_{\text{Cu}(\text{OH})} = \frac{[\text{Lu}(\text{L})\text{Cu}(\text{OH})]K_{\text{w}}}{[\text{Lu}(\text{L})\text{Cu}][\text{H}^+]} \quad (6)$$

$$k_{\text{obs}} = \frac{k_0 + k_1[\text{H}^+] + k_3[\text{Cu}^{2+}] + k_6[\text{Cu}^{2+}]K_{\text{w}}/[\text{H}^+]}{1 + K_{\text{H}}[\text{H}^+] + K_{\text{Cu}}[\text{Cu}^{2+}] + K_{\text{Cu}(\text{OH})}K_{\text{Cu}}[\text{Cu}^{2+}]K_{\text{w}}/[\text{H}^+]} \quad (7)$$

Attempts to fit the data to eq 7 including  $k_0$  as fitting parameter provided a small negative value, which indicates that spontaneous dissociation does not play any role under the conditions used for kinetic experiments. Furthermore, it is difficult to estimate the rate constant characterizing the spontaneous reaction pathway within the same pH range where the dissociation of the  $\text{Lu}(\text{L})\text{Cu}(\text{OH})$  complex takes

**Table 4.** Rate and Equilibrium Constants Characterizing the Dissociation of the  $\text{CHXOCTAPA}^{4-}$  Complexes and Related Systems (25 °C)

	$[\text{LuCHXOCTAPA}]^-$	$[\text{GdCHXOCTAPA}]^-^a$	$[\text{GdOCTAPA}]^-^b$	$[\text{GdDTPA}]2^-^c$	$[\text{GdDO3A}]^d$
$k_1/\text{M}^{-1} \text{s}^{-1}$	$3.74 \pm 0.06 \times 10^{-2}$	$1.60 \times 10^{-2}$	11.8	0.58	0.023
$k_2/\text{M}^{-2} \text{s}^{-2}$			$2.5 \times 10^4$	$9.7 \times 10^4$	
$k_3^{\text{Cu}}/\text{M}^{-1} \text{s}^{-1}$	$6.3 \pm 0.3 \times 10^{-4}$	$6.8 \times 10^{-4}$	22.5	0.93	
$k_6^{\text{Cu}}/\text{M}^{-2} \text{s}^{-1}$	$5.1 \pm 0.3 \times 10^5$		$5.0 \times 10^9$		
$K_{\text{H}}$		737	2.6	100	
$K_{\text{Cu}}$	$12.1 \pm 1.6$	48		13	
$t_{1/2}/\text{h}^e$	876	$1.49 \times 10^5$	0.15	202	$2.10 \times 10^5$

<sup>a</sup>Data from ref 38. <sup>b</sup>Data from ref 26. <sup>c</sup>Data from ref 25. <sup>d</sup>Data from ref 47. <sup>e</sup>Half-lives determined at pH 7.4 and  $[\text{Cu}^{2+}] = 1 \mu\text{M}$ .



place, as the latter acts as a competitive dissociation path to the spontaneous dissociation. A similar situation occurred for  $K_{\text{H}}$ , revealing that the  $K_{\text{H}}[\text{H}^+]$  term in the denominator of eq 7 has a negligible contribution to  $k_{\text{obs}}$ . This is expected considering the low protonation constants determined using potentiometry (log  $K_{\text{LnH}}$  in the range 1–2, Table 1) and the relatively low proton concentrations used for kinetic experiments ( $<10^{-6}$  M, Figure 6). The results of the fit are shown in Table 4, together with a comparison with the data reported previously for the  $\text{Gd}^{3+}$  complexes of  $\text{CHXOCTAPA}^{4-}$ ,<sup>38</sup>  $\text{OCTAPA}^{4-}$ ,<sup>31</sup>  $\text{DTPA}^{5-}$ ,<sup>25</sup> and  $\text{DO3A}^{3-}$ .<sup>47</sup> It is worth mentioning that the dissociation pathway through formation of a hydroxo dinuclear species was not detected for the  $\text{Gd}^{3+}$  analogue, which was investigated in approximately the same pH range. The formation of hydroxo complexes is more likely to occur as the size of the lanthanide ion decreases across the series due to the lanthanide contraction, as indicated by the corresponding hydrolysis constants (log  $K_{\text{Ln(OH)}} = -7.83$  and  $-7.27$  for  $\text{Gd}^{3+}$  and  $\text{Lu}^{3+}$ , respectively).<sup>99</sup> Alternatively, the structural change occurring close to the center of the lanthanide series could be responsible for the different behavior of the  $\text{Gd}^{3+}$  and  $\text{Lu}^{3+}$  complexes.

The rate constants shown in Table 4 indicate that the  $\text{Gd}^{3+}$  and  $\text{Lu}^{3+}$  analogues present similar inertness with respect to their dissociation following the proton-assisted and metal-assisted pathways, as judged by the values of the  $k_1$  and  $k_3^{\text{Cu}}$  rate constants. However, the metal-assisted pathway with the formation of a hydroxo complex, characterized by  $k_6^{\text{Cu}}$ , plays an increasingly important role in the dissociation of the complex as the concentration of  $\text{OH}^-$  increases. As a result, this pathway is mainly responsible for complex dissociation at pH 7.4, a situation that is clearly reflected in the half-lives of the complex calculated at pH 7.4 using  $[\text{Cu}^{2+}] = 1 \mu\text{M}$  (Table 4). Nevertheless, the half-life estimated for  $[\text{Lu}(\text{CHXOCTAPA})]^-$  remains three times longer than that of  $[\text{Gd}(\text{DTPA})]^{2-}$ , but clearly shorter than that of the macrocyclic complex  $[\text{Gd}(\text{DO3A})]$ . The effect that the rigid cyclohexyl unit has in improving kinetic inertness is also obvious when comparing the half-lives of  $\text{CHXOCTAPA}^{4-}$  and  $\text{OCTAPA}^{4-}$  derivatives.

## CONCLUSIONS

The present contribution has shown that the octadentate  $\text{CHXOCTAPA}^{4-}$  ligand forms fairly stable complexes with the  $\text{Ln}^{3+}$  ions, with stability constants in the range log  $K_{\text{LnL}} \sim 17.8$ – $19.7$ . The presence of the rigid cyclohexyl ring causes a slight increase of the selectivity of the ligand for the  $\text{Ln}^{3+}$  ions over  $\text{Cu}^{2+}$  and  $\text{Zn}^{2+}$ . The picolinate units are rather efficient in sensitizing the  $\text{Eu}^{3+}$  and particularly  $\text{Tb}^{3+}$  luminescence, with emission quantum yields comparable to those of the  $\text{OCTAPA}^{4-}$  analogues. The complexes are monohydrated ( $q = 1$ ) in solution, as indicated by emission lifetime measurements. The exchange rate of the water molecule coordinated to  $\text{Gd}^{3+}$  (as confirmed by  $^{17}\text{O}$  NMR studies) is rather low when compared with the  $\text{OCTAPA}^{4-}$ ,  $\text{DTPA}^{5-}$ , and  $\text{DOTA}^{4-}$  analogues, likely as a result of the rigid structure of the complex.

The coordination chemistry reported in this paper provided two unexpected results. First, the analysis of the structural information encoded by the pseudocontact shifts, induced by  $\text{Yb}^{3+}$ , demonstrate that this complex presents an unusual cis structure in which the amine N atoms adopt *S,R* configurations. DFT calculations show that this conformation is

stabilized across the lanthanide series over the *trans R,R* (or *S,S*) conformation. The presence of the cyclohexyl group causes a significant stabilization of the *S,R* conformation. A second unexpected effect was observed when investigating the dissociation of the  $\text{Lu}^{3+}$  complex in the presence of exchanging  $\text{Cu}^{2+}$  ions. Complex dissociation at physiological pH was found to occur mainly through the metal-assisted mechanism that involves the formation of a hydroxo complex, a pathway that was not observed previously for the  $\text{Gd}^{3+}$  analogue. We hypothesize that this pathway may be relevant for the dissociation of complexes of acidic cations relevant for radiopharmaceutical applications (i.e.,  $\text{Sc}^{3+}$ ).

## EXPERIMENTAL AND COMPUTATIONAL SECTION

**Materials.** The  $\text{H}_4\text{CHXOCTAPA}$  and  $\text{H}_4\text{OCTAPA}$  ligands were prepared as described in previous papers.<sup>31,38</sup> All other chemicals and solvents were purchased from commercial sources and used without further purification. The complexes used for NMR and photophysical studies were prepared by mixing stoichiometric amounts of the ligand and the corresponding  $\text{Ln}(\text{OTf})_3$  salts and subsequent adjustment of the pH with diluted  $\text{NaOH}/\text{NaOD}$  solutions.

**NMR Spectroscopy.**  $^1\text{H}$  NMR spectra were recorded at 25 °C in solutions of the complexes in  $\text{D}_2\text{O}$  using Bruker Avance 300 or Bruker ARX400 spectrometers. Chemical shifts were referenced by using the residual solvent HDO proton signal ( $\delta = 4.79$  ppm).<sup>100</sup>

The  $^1\text{H}$  NMRD measurements were carried out by using a Stelar SMARTracer Fast Field Cycling relaxometer (0.01–10 MHz) and a Bruker WP80 NMR electromagnet adapted to variable field measurements (20–80 MHz) controlled by a SMARTracer PC-NMR console. The NMRD profiles of the  $[\text{Gd}(\text{CHXOCTAPA})]^-$  complex ( $c_{\text{complex}} = 2.69$  mM) were recorded in aqueous solution at three different temperatures (25, 37 and 50 °C) in the presence of 4-(2-hydroxyethyl)-1-piperazineethanesulfonic acid buffer (25 mM, pH = 7.27) to maintain the pH constant. The temperature of the samples was managed by a VTC91 temperature control unit (calibrated by a Pt resistance temperature probe) and maintained by gas flow.

Transverse and longitudinal  $^{17}\text{O}$  relaxation rates ( $1/T_2$ ,  $1/T_1$ ) and chemical shifts were measured in aqueous solutions of  $[\text{Gd}(\text{CHXOCTAPA})]^-$  (0.0199 mM, pH = 7.27) in the temperature range 274–354 K on a Bruker Avance 400 (9.4 T, 54.24 MHz) spectrometer. The temperature was calculated according to previous calibration with ethylene glycol and methanol.<sup>101</sup> An acidified water solution ( $\text{HClO}_4$ , pH 3.3) was used as an external reference. Longitudinal relaxation times ( $T_1$ ) were obtained by the inversion–recovery method, and transverse relaxation times ( $T_2$ ) were obtained by the Carr–Purcell–Meiboom–Gill spin-echo technique.<sup>102</sup> The technique used for  $^{17}\text{O}$  NMR measurements on  $\text{Gd}^{3+}$  complexes has been described elsewhere.<sup>103</sup> The samples were sealed in glass spheres fitted into 10 mm NMR tubes to avoid susceptibility corrections of the chemical shifts.<sup>104</sup> To improve the sensitivity,  $^{17}\text{O}$ -enriched water (10%  $\text{H}_2^{17}\text{O}$ , CortecNet) was added to the solutions to reach around 2% enrichment. The  $^{17}\text{O}$  NMR data were treated according to the Solomon–Bloembergen–Morgan theory of paramagnetic relaxation. The least-squares fit of the  $^{17}\text{O}$  NMR and  $^1\text{H}$  NMRD data was performed using Micromath Scientist version 2.0 (Salt Lake City, UT, USA).

**Absorption and Emission Electronic Spectroscopy.** The absorption spectra of the  $\text{Eu}^{3+}$  and  $\text{Tb}^{3+}$  complexes were recorded with a Jasco V-650 spectrometer using 0.2 cm quartz cells. Steady-state emission spectra were obtained with a Horiba FluoroMax Plus-P spectrofluorometer using a 150 W ozone-free xenon arc lamp as the excitation source, a R928P photon counting emission detector, and an integration time of 0.1 s. Luminescence lifetimes were measured using the time-correlated single photon counting technique and a pulsed xenon flash lamp as the excitation source. Quantum yields were determined using the  $\text{Cs}_3[\text{Ln}(\text{pic})_3]$  complexes (pic = 2,6-dipicolinate, Ln = Eu or Tb) as standards ( $\Phi_{\text{Eu}} = 24\%$  in TRIS, pH 7.4,  $7.5 \times 10^{-5}$  M;  $\Phi_{\text{Tb}} = 22\%$  in TRIS, pH 7.4,  $6.5 \times 10^{-5}$  M).<sup>52,53</sup>











(117) Visscher, L.; Dyall, K. G. Dirac–Fock Atomic Electronic Structure Calculations Using Different Nuclear Charge Distributions. *At. Data Nucl. Data Tables* **1997**, *67*, 207–224.

(118) Tao, J.; Perdew, J. P.; Staroverov, V. N.; Scuseria, G. E. Climbing the Density Functional Ladder: Nonempirical Meta–Generalized Gradient Approximation Designed for Molecules and Solids. *Phys. Rev. Lett.* **2003**, *91*, 146401.

(119) Esteban-Gómez, D.; de Blas, A.; Rodríguez-Blas, T.; Helm, L.; Platas-Iglesias, C. Hyperfine Coupling Constants on Inner-Sphere Water Molecules of Gd<sup>III</sup>-Based MRI Contrast Agents. *ChemPhysChem* **2012**, *13*, 3640–3650.

(120) Kossmann, S.; Kirchner, B.; Neese, F. Performance of Modern Density Functional Theory for the Prediction of Hyperfine Structure: Meta-GGA and Double Hybrid Functionals. *Mol. Phys.* **2007**, *105*, 2049–2071.

(121) Reiher, M. Douglas–Kroll–Hess Theory: A Relativistic Electrons-Only Theory for Chemistry. *Theor. Chem. Acc.* **2006**, *116*, 241–252.

(122) Barysz, M.; Sadlej, A. J. Two-Component Methods of Relativistic Quantum Chemistry: From the Douglas–Kroll Approximation to the Exact Two-Component Formalism. *J. Mol. Struct.: THEOCHEM* **2001**, *573*, 181–200.

(123) Aravena, D.; Neese, F.; Pantazis, D. A. Improved Segmented All-Electron Relativistically Contracted Basis Sets for the Lanthanides. *J. Chem. Theory Comput.* **2016**, *12*, 1148–1156.

(124) Weigend, F.; Ahlrichs, R. Balanced Basis Sets of Split Valence, Triple Zeta Valence and Quadruple Zeta Valence Quality for H to Rn: Design and Assessment of Accuracy. *Phys. Chem. Chem. Phys.* **2005**, *7*, 3297.

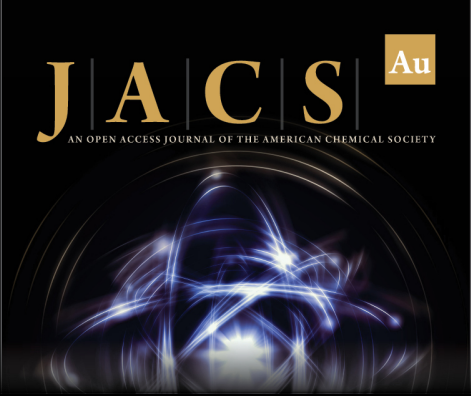
(125) Kossmann, S.; Neese, F. Comparison of Two Efficient Approximate Hartree–Fock Approaches. *Chem. Phys. Lett.* **2009**, *481*, 240–243.

(126) Neese, F.; Wennmohs, F.; Hansen, A.; Becker, U. Efficient, Approximate and Parallel Hartree–Fock and Hybrid DFT Calculations. A ‘Chain-of-Spheres’ Algorithm for the Hartree–Fock Exchange. *Chem. Phys.* **2009**, *356*, 98–109.


(127) Stoychev, G. L.; Auer, A. A.; Neese, F. Automatic Generation of Auxiliary Basis Sets. *J. Chem. Theory Comput.* **2017**, *13*, 554–562.


(128) Weigend, F. Accurate Coulomb-Fitting Basis Sets for H to Rn. *Phys. Chem. Chem. Phys.* **2006**, *8*, 1057–1065.


(129) Marenich, A. V.; Cramer, C. J.; Truhlar, D. G. Universal Solvation Model Based on Solute Electron Density and on a Continuum Model of the Solvent Defined by the Bulk Dielectric Constant and Atomic Surface Tensions. *J. Phys. Chem. B* **2009**, *113*, 6378–6396.



**JACS** <sup>Au</sup>  
AN OPEN ACCESS JOURNAL OF THE AMERICAN CHEMICAL SOCIETY

 Editor-in-Chief  
**Prof. Christopher W. Jones**  
Georgia Institute of Technology, USA

**Open for Submissions** 

pubs.acs.org/jacsau  ACS Publications  
Most Trusted. Most Cited. Most Read.